



**UNIVERSITY POLITEHNICA of BUCHAREST**

Faculty of Mechanical Engineering and Mechatronics

Thermodynamics, Heat engines, Thermal and Refrigerating Equipment

# **PH.D. THESIS**

**CONTRIBUTIONS TO THE OPTIMIZATION OF CRYOGENIC GAS  
SEPARATION INSTALLATIONS**

**Author:** Eng. Sorin Bucșa

**Scientific advisor:** Ph.D. Professor Alexandru Șerban

Bucharest

2021

# CONTENT

CHAPTER 1. CURRENT STAGE OF RESEARCH IN THE FIELD	3
1.1. INTRODUCTION TO THE SEPARATION OF INDUSTRIAL GASES BY CRYOGENIC PROCESSES	3
1.2. AIR COMPRESSION IN CRYOGENIC SEPARATION INSTALLATIONS	4
<b>CHAPTER 2. THE THERMODYNAMIC GAS SEPARATION PROCESS</b>	<b>12</b>
<b>CHAPTER 3. EXERGETIC ANALYSIS OF THE CRYOGENIC AIR SEPARATION INSTALLATION</b>	<b>27</b>
3.1. INTRODUCTION	<b>ERROR! BOOKMARK NOT DEFINED.</b>
3.2. THE ENVIRONMENT	<b>ERROR! BOOKMARK NOT DEFINED.</b>
3.3. THE DEAD STATE	<b>ERROR! BOOKMARK NOT DEFINED.</b>
3.4. THERMO-MECHANICAL EXERGY	6
3.5. CHEMICAL EXERGY	8
<b>CHAPTER 4. EXERGETIC ANALYSIS OF A CRYOGENIC AIR SEPARATION INSTALLATION</b>	<b>38</b>
4.1. DESCRIPTION OF THE INSTALLATION. FUNCTIONAL SCHEME	<b>ERROR! BOOKMARK NOT DEFINED.</b>
4.2. EXERGETIC ANALYSIS	11
4.3. COMPRESSION AREA	12
4.4. HIGH PRESSURE DISTILLATION COLUMN (HPC)	13
4.5. LOW PRESSURE DISTILLATION COLUMN (LPC)	15
4.6. RESULTS AND DISCUSSIONS	16
4.6.1. <i>Compression area</i>	17
4.6.2. <i>High pressure distillation column HPC</i>	18
4.6.3. <i>Low pressure distillation column LPC</i>	<b>Error! Bookmark not defined.</b>
<b>CHAPTER 5. EXERETIC ANALYSIS OF THE COMPRESSION ZONE</b>	<b>72</b>
5.1. COMPRESSION STAGE	<b>ERROR! BOOKMARK NOT DEFINED.</b>
5.2. CHOICE OF INTERMEDIATE CHILLERS AND FINAL COOLER ON THE BASIS OF OPTIMUM ENTROPY GENERATION (OPTIMUM EXERGY DESTRUCTION)	20
5.2.1. <i>Thermal efficiency of a heat exchanger</i>	<b>Error! Bookmark not defined.</b>
5.2.2. <i>Number of heat transfer units NTU</i>	<b>Error! Bookmark not defined.</b>
5.2.3. <i>Destruction of exergy in the cooler</i>	20
5.2.4. <i>Sizing of the first intermediate chiller based on the NEU number of destroyed exergy units</i>	<b>Error!</b>
	<b>Bookmark not defined.</b>
<b>CHAPTER 6. ATTEMPTS FOR INCREASING THE PERFORMANCE OF CRYOGENIC AIR SEPARATION INSTALLATIONS</b>	<b>83</b>
6.1 HEAT RECOVERY POTENTIAL DISCHARGED FROM THE CRYOGENIC AIR SEPARATION PLANT FROM THE GALAȚI STEEL PLANT	85
6.2 RANKINE CYCLES WITH ORGANIC FLUIDS	85
6.2.1. <i>Organic fluids</i>	<b>Error! Bookmark not defined.</b>
6.2.2. <i>Comparison between ORC cycles and Rankine steam cycle</i>	<b>Error!</b>
	<b>Bookmark not defined.</b>
6.3. THERMODYNAMIC ANALYSIS OF ORC CYCLES	<b>ERROR! BOOKMARK NOT DEFINED.</b>
6.3.1. <i>ORC cycle with non-negative vapor saturation curve slope without vapor overheating at the inlet to the expander and without internal recuperator heat exchanger</i>	<b>Error!</b>
	<b>Bookmark not defined.</b>

6.3.2.	<i>Non-negative ORC cycle with vapor saturation curve slope, without vapor overheating at the inlet to the expander, with internal heat exchanger.</i>	<b>Error! Bookmark not defined.</b>
6.3.3.	<i>ORC cycle with non-negative vapor saturation curve slope with vapor overheating at the inlet to the expander and with recuperative internal heat exchanger</i>	<b>Error! Bookmark not defined.</b>
6.3.4.	<i>Mathematical modeling of the ORC cycle</i>	22
6.4.	EXERGETIC ANALYSIS	23
6.5.	STUDY OF THE PERFORMANCE OF THE ORC CYCLE WORKING WITH DIFFERENT ORGANIC SUBSTANCES	<b>Error!</b>
	<b>Bookmark not defined.</b>	
6.5.1.	<i>Study of the performance of the ORC cycle operating with R-245fa</i>	<b>Error! Bookmark not defined.</b>
6.5.2.	<i>Comparative study of the performances of the ORC cycle working with different organic fluids</i>	<b>Error! Bookmark not defined.</b>
	<b>Error! Bookmark not defined.</b>	
	FINAL CONCLUSIONS AND PERSONAL CONTRIBUTIONS .....	<b>ERROR! BOOKMARK NOT DEFINED.</b>
	LIST OF FIGURES .....	<b>ERROR! BOOKMARK NOT DEFINED.</b>
	BIBLIOGRAPHY.....	<b>ERROR! BOOKMARK NOT DEFINED.</b>

## CHAPTER 1. CURRENT STAGE OF RESEARCH IN THE FIELD

### 1.1 Introduction to the separation of industrial gases by cryogenic processes

The foundations of low temperature liquefaction and natural gas separation are based on scientific principles and technologies of cryogenic engineering, which developed fully in the eighteenth century. In 1703, the work in the field of thermometry and mathematics, by the French physicist Guillaume Amontons, led to the notion of an absolute zero. In addition, in 1720, Gabriel Daniel Fahrenheit developed the idea of the temperature scale that bears his name.

In the 19th century, attempts were made to liquefy industrial gases and their behavior and characteristics were studied. In 1823, Michael Faraday liquefied chlorine and studied the liquefaction and properties of ammonia.

In 1845, the Scotsman Thomas Andrews conducted an experiment involving the phase change of carbon dioxide at different temperatures and pressures, generating the first isotherms. They show that a gas, regardless of pressure, can only be liquefied if it is first cooled to or below the critical temperature. [2]

In 1865, engineer Carl Linde designed a refrigeration machine based on the Carnot Cycle and achieved low temperatures by vapor compression. Linde also built the first industrial air liquefaction machine in 1895, using the same principle and a countercurrent spiral heat exchanger (designed by William Hampson).

In 1882, at the University of Leyden, the Netherlands, Keike Kamerlingh Onnes set up the cryogenics laboratory to study the equations of state, isotherms and general thermodynamic properties of cryogenic liquids and gases.

Since the beginning of the twentieth century, cryogenic air separation units (Air Separation Unit - ASU) have been used to separate air into its constituents, mainly oxygen, nitrogen and argon in various purities, states and quantities.

Since the beginning of the twentieth century, cryogenic air separation units (Air Separation Unit - ASU) have been used to separate air into its constituents, mainly oxygen, nitrogen and argon in various purities, states and quantities.

Applications of oxygen under pressure can be found in agriculture, chemical processing, petrochemicals, oil and gas production, oil refining and the glass industry [28], [29]. Since the advent of the L-D (Linz – Donawitz) steelmaking process in the early 1950s, the capacity of air separation plants has greatly increased. Since producing two tons per day, a single ASU now produces 5,000 tons per day of oxygen [30].

## 1.2 Air compression in cryogenic separation plants

The cryogenic air separation plant is a capital and energy intensive process. In a typical cryogenic ASU (Air Separation Unit), the atmospheric air must be cleaned, compressed and cooled to about  $-180^{\circ}\text{C}$ , the liquefied stream is then distilled in a large distillation tower to separate the air into its components. The energy consumption of cryogenic ASU comes mainly from the energy requirement of the air supply compressor.

Energy efficiency is an important measure of performance in industrial installations.

Energy efficiency has been applied to different energy systems to evaluate and compare them, thus finding opportunities to improve processes. Such definitions of energy efficiency depend on the case-by-case characteristics of a process, which means that there is no general mathematical expression for energy efficiency [61] [62] [63]. This can lead to misinterpretations in the definitions of energy efficiency and can produce inconsistent results even for the same system. Thus, an objective performance parameter is needed for energy conversion efficiency. Another limitation of energy efficiency is that it does not take energy quality into account when measuring process performance. Different forms of energy have different qualities, for example, the value of heat cannot be directly compared to the value of power, because the quality of heat energy will vary, depending on the temperature level. Unlike energy analysis, exergy gives both the quantity and quality of different forms of energy, which is why exergy has been recommended as a measure of system performance [65]. Exergy is the potential to produce mechanical work, so the destruction or loss of exergy can be considered a loss of mechanical work potential [37].

Many efforts have been made to reduce the costs and energy consumption of cryogenic installations from air separation. The exergetic analysis performed by Fu and Gundersen [81] indicated that the air compression process is characterized by an exergy loss of 38.4% of the total electricity consumption.

Many research efforts have been made to recover heat waste from air compression in recent years. The most common method is the direct reuse of residual heat by compression to meet

specific thermal requirements for other processes, such as space heating [89], hot water production for industrial and household applications [90] - [92], dehumidification regeneration dehydrating substances [93] etc

Air compression performance is crucial for the overall efficiency of cryogenic air separation units [88]. Air separation units (ASUs), as a single industrial equipment, accounted for a considerable proportion (4.97%) of China's total national power consumption [95], which ranks first in steel production.

## CHAPTER 2. THE THERMODYNAMIC GAS SEPARATION PROCESS

If in the case of gas mixing one could collect mechanical work released by expanding each component from its initial pressure to its partial pressure in the mixture and this mechanical work produced would be sufficient for the separation on components of the mixture - mixing process - separation would be reversible.

In the case of a mixture of  $m$  components, the minimum mechanical work required to separate all  $m$  components of a mole of mixture at ambient pressure  $p_0$  and temperature  $T_0$ , becomes:

$$\frac{[L^{min}]}{n} = T_0 \left\{ \sum_{i=1}^m r_i [\bar{s}_i(T_0, r_i \cdot p_0) - \bar{s}_1(T_0, p_0)] \right\} - \sum_{i=1}^m r_i [\bar{h}_i(T_0, r_i \cdot p_0) - \bar{h}_i(T_0, p_0)] \left[ \frac{J}{mol \text{ mix}} \right] \quad (2.8)$$

If only one component ( $k$ ) is separated and the remaining components remain unmixed, the minimum mechanical separation work for one mole of mixture shall be calculated by the expression:

$$\frac{[L_k^{min}]}{n} = T_0 \left\{ r_k [\bar{s}_k(T_0, r_k \cdot p_0) - \bar{s}_k(T_0, p_0)] + (1 - r_k) \left[ \sum_{i=1}^{m \text{ f\u0103r\u0103 } k} r'_i [\bar{s}_i(T_0, r_i \cdot p_0)] - \bar{s}_i(T_0, p_0) \right] \right\} - \left\{ r_k [\bar{h}_k(T_0, r_k \cdot p_0) - \bar{h}_k(T_0, p_0)] + (1 - r_k) \left[ \sum_{i=1}^{m \text{ f\u0103r\u0103 } k} r'_i [\bar{h}_i(T_0, r_i \cdot p_0)] - \bar{h}_i(T_0, p_0) \right] \right\} \left[ \frac{J}{mol \text{ mix}} \right] \quad (2.9)$$

Table 2.2 shows the values of the minimum mechanical work consumed to separate each component from the dry air when the air is completely separated into its components.

Table 2. 1. Minimum mechanical work for separation (MMLS) of each component of dry air when the air is completely separated in its component gases at  $T_0 = 300K$

Gas in the dry air		Molar composition in the dry air [mol/mol air]	MMLS in component gases for one mol of dry air [J/mol air]	MMLS of a mol of a component gas [J/mol]	MMLS of a gram of a component gas [J/g]
Nume	Formula chimic\u0103				
Azot	N <sub>2</sub>	0,78084	1417	1815	64,78
Oxigen	O <sub>2</sub>	0,20946		6765	211,4
Argon	Ar	9,34x10 <sup>-3</sup>		151714	3798
Dioxid de carbon	CO <sub>2</sub>	3,3x10 <sup>-4</sup>		4,294E+06	97568

Neon	Ne	$1,818 \times 10^{-5}$		7,794E+07	3,862E+06
Heliu	He	$5,24 \times 10^{-6}$		2,933E+07	7,328E+06
Metan	CH <sub>4</sub>	$1,79 \times 10^{-6}$		7,916E+08	4,935E+07
Krypton	Kr	$1 \times 10^{-6}$		1,417E+09	1,691E+07
Hidrogen	H <sub>2</sub>	$5 \times 10^{-7}$		2,834E+09	1,46E+09
Xenon	Xe	$9 \times 10^{-8}$		1,574E+10	1,199E+08

Table 2.3 shows the values of the minimum mechanical work consumed to separate one of the components while the others remain mixed.

Table 2.3. Minimum mechanical work for separation (MMLS) of each component in dry air when the remaining component gases remain mixed at  $T_0 = 300\text{K}$

Gas in the dry air		Molar composition in the dry air [mol/mol air]	MMLS to separate one gas component from one mol of dry air [J/mol aer]	MMLS of a mol of gas component [J/mol]	MMLS of a gram of a gas component [J/g]
Name	Chemical formula				
Azot	N <sub>2</sub>	0,78084	1312	1680	59,96
Oxigen	O <sub>2</sub>	0,20946	1280	6112	191
Argon	Ar	$9,34 \times 10^{-3}$	132,1	14140	353,9
Dioxid de carbon	CO <sub>2</sub>	$3,3 \times 10^{-4}$	7,421	22489	511
Neon	Ne	$1,818 \times 10^{-5}$	0,5403	29720	1473
Heliu	He	$5,24 \times 10^{-6}$	1,318	27282	6815
Metan	CH <sub>4</sub>	$1,79 \times 10^{-6}$	0,06355	35502	2213
Krypton	Kr	$1 \times 10^{-6}$	0,03695	36954	441
Hidrogen	H <sub>2</sub>	$5 \times 10^{-7}$	0,01934	38683	19188
Xenon	Xe	$9 \times 10^{-8}$	0,003866	42960	327,2

## CHAPTER 3. EXERGETIC ANALYSIS OF THE CRYOGENIC AIR SEPARATION INSTALLATION

The viable study method for identifying malfunctions within the system must also be based on the second principle of thermodynamics which brings the concept of entropy generation as a measure of transforming an ordered amount of energy into an unordered energy while obviously maintaining quantitative equivalence

The exergy of a certain amount of energy is determined according to the intensive parameters of the environment (thermal - temperature  $T_0$ , mechanical - pressure  $p_0$  and chemical - the chemical potential of components  $k$  that make up the environment reference environment  $\mu_k^0$ ).

### 3.4 Thermo-mechanical exergy

The significance of the thermal or mechanical exergy depends on the value of the temperature or pressure of the heat source or of the substance current in relation to the temperature  $t_0$  and the pressure  $p_0$  of the environment.

In all cases in order to highlight the thermal and mechanical exergy of the system the system must be brought to the reference state which is the restrictive dead state.

If:

$T > T_0$	the exergy $Ex_Q^T$ of a quantity Q of heat at temperature T represents the maximum mechanical work that could be produced by a direct Carnot cycle operating between temperatures T și $T_0$
$p > p_0$	the exergia Ex of a current of substance in flow represents the maximum mechanical work that could be produced by a reversible expansion from p to $p_0$
$T < T_0$	the exergy $ Ex_Q^T $ represents the minimum work consumed by an inverse Carnot cycle when transporting the heat Q from the temperature level T to $T_0$
$p < p_0$	exergy Ex of a flowing current of substance represents the minimum mechanical work required for a reversible compression from p to $p_0$

The thermo-mechanical exergy of an open system (control volume) called flow exergy [100] is calculated with the relationship:

$$Ex_{vc} = (H - H_0) - T_0(S - S_0) + \frac{m \cdot w^2}{2} + m \cdot g \cdot z \quad (3.4)$$

The heat exergy is:

$$Ex_Q^T = Q \left(1 - \frac{T_0}{T}\right) \quad (3.5)$$

The exergetic balance equations written by an observer outside the system, accounting for interactions in steady state at the boundary separating the system from its environment become:

a) Closed system (control mass)

$$\sum Ex_Q = \Delta Ex + \left(\sum L - p_0 \cdot \Delta V\right) + \sum I \quad (3.6)$$

in which I represents the destruction of exergy due to the internal irreversibility of the processes.

b) Open system (control volume)

$$\sum \dot{Ex}_Q = \sum \dot{m}_e \cdot ex_e - \sum \dot{m}_i \cdot ex_i + \sum \dot{L} + \sum \dot{I} \quad (3.7)$$

Exergy destruction I can be calculated from the exergetic balance equation as the only term that cannot be measured at the outer surface of the boundary between the system and its external environment (where the observer is located) or based on the Gouy-Stodola theorem [101] - [103]:

$$\dot{I} = T_0 \cdot \dot{S}_{gen} \quad (3.8)$$

In steady state the entropy generation inside the contro volume becomes:

$$\dot{S}_{gen} = \sum \dot{m}_e \cdot s_e - \sum \dot{m}_i \cdot s_i - \sum \frac{\dot{Q}_j}{T_j} \quad (3.9)$$

where indices e and i refer to the output and input currents, respectively.

### 3.5 Chemical exergy

The general expression of the chemical exergy is obtained by extracting from the total exergy the thermo-mechanical exergy.

$$\begin{aligned} Ex^{CH} &= Ex^{TOT} - Ex^{TM} \\ &= E + p_0 \cdot V - T_0 \cdot S - \sum_{k=1}^n n_k \cdot \mu_k^0 - \left( E + p_0 \cdot V - T_0 \cdot S - \sum_{k=1}^n n_k \cdot \mu_{k0} \right) \\ Ex^{CH} &= \sum_{k=1}^n n_k \cdot \mu_{k0} - \sum_{k=1}^n n_k \cdot \mu_k^0 = \sum_{k=1}^n n_k (\mu_{k0} - \mu_k^0) \end{aligned} \quad (3.38)$$

In the case of total exergy of a cryogenic liquid resulting from the separation of air, in the state of thermo-mechanical equilibrium with the environment ( $T = T_0$  and  $p = p_0$ ) the substance is in the gaseous state.

If the liquid in component k is initially at  $p_1, T_1$ , by bringing it reversibly to thermo-mechanical equilibrium with the environment, its thermo-mechanical exergy is highlighted.

In order to release the chemical exergy, the gas expands isothermally reversible at temperatures  $T_0$  in a turbine, from the pressure  $p_0$  to its partial pressure in the ambient environment  $p_k^0$ .

$$\begin{aligned} Ex_k^{TOT} &= n_k \{ \bar{h}_1(p_1, T_1) - \bar{h}_0(p_0, T_0) - T_0 [\bar{s}_1(p_1, T_1) - \bar{s}_0(p_0, T_0)] \} + n_k \cdot \bar{R} \cdot T_0 \cdot \ln \frac{p_0}{p_k^0} = \\ &= n_k \left\{ \bar{h}_1(p_1, T_1) - \bar{h}_0(p_0, T_0) - T_0 [\bar{s}_1(p_1, T_1) - \bar{s}_0(p_0, T_0)] + \bar{R} \cdot T_0 \cdot \ln \frac{1}{r_k^0} \right\} \end{aligned} \quad (3.46)$$

where

$$Ex_k^{TM} = n_k \{ \bar{h}_1(p_1, T_1) - \bar{h}_0(p_0, T_0) - T_0 [\bar{s}_1(p_1, T_1) - \bar{s}_0(p_0, T_0)] \} \quad (3.47)$$

$$Ex_k^{CH} = n_k \cdot \bar{R} \cdot T_0 \cdot \ln \frac{1}{r_k^0} \quad (3.48)$$

The chemical exergences of the component gases of the ambient dry air whose composition is shown in Table (a.1) are given in Table (3.1).

Table 3.1. Chemical exergies of the component gases of the surrounding dry air ( $T_0 = 298 \text{ K}$ )

Dry air composition		Volumetric composition = molar composition in the dry air		Molar Chemical Exergy $\bar{e}_x^{CH}$
Name	Formula	[mol/mol <sub>aer</sub> ]	[%]	[J/mol]
Azot	N <sub>2</sub>	0.78084	78.084	612,95
Oxygen	O <sub>2</sub>	0.20946	20.946	3873,23
Argon	Ar	0.00934	0.934	11579,5
Dioxid de carbon	CO <sub>2</sub>	0.00033	0.033	19862,45
Neon	Ne	0.00001818	0.001818	27055,72
Helium	He	0.00000524	0.000524	30146
Metan	CH <sub>4</sub>	0.00000179	0.000179	32774,6
Kripton	Kr	0.0000010	0.0001	34230,98
Hidrogen	H <sub>2</sub>	0.0000005	0.00005	35948,4
Xenon	Xe	0.00000009	0.000009	
<b>Universal constant of gases <math>\bar{R} = 8,3145 \left[ \frac{\text{J}}{\text{mol}\cdot\text{K}} \right]</math></b>				

The comparison of expressions (3.47) and (a.13) shows that the minimum mechanical separation work at temperature  $T_0$  of a gaseous mixture is equal to the sum of the chemical exergies of the component gases.

## CHAPTER 4. EXERGETIC ANALYSIS OF A CRYOGENIC AIR SEPARATION INSTALLATION

### 4.1. DESCRIPTION OF THE INSTALLATION. FUNCTIONAL SCHEME

The case study analyzes the cryogenic installation from the air separation on the platform of the Arcelor Mittal Steel Plant in Galați.

The installation processes an air flow  $\dot{V}_{aer} = 363000 \left[ \frac{\text{m}^3\text{N}}{\text{h}} \right]$  ensuring an oxygen gas production  $\dot{V}_{O_2} = 58300 \left[ \frac{\text{m}^3\text{N}}{\text{h}} \right]$  with a concentration greater than 98.5%.

The scheme of the installation is presented in figure 4.1

The separation of the air is done in two distillation columns that operate at different pressures coupled by a heat exchanger acting as a condenser for the high pressure column (HPC) and evaporator (reboiler) for the low pressure column (LPC). HPC operates at a pressure of about 6 bar and LPC at about 1.4 bar [104], [105].

The compressed, dry and purified atmospheric air is cooled in the main recuperative heat exchanger to close to its liquefaction temperature ( $-170^{\circ}\text{C}$ ) and introduced into the high pressure column (HPC).

In the high pressure column (HPC) the air is separated by distillation into a stream of nitrogen gas which accumulates at the top of the column and a stream of oxygen-enriched liquid (about 30%  $\text{O}_2$ ) at the bottom.

The separation process is repeated in the low-pressure column (LPC).

The nitrogen gas in the high pressure (and temperature) (HPC) column is partially condensed in the evaporator condenser that couples the two columns by transferring heat to the oxygen-enriched liquid in the low-pressure column (LPC) which vaporizes at about  $-180^{\circ}\text{C}$ .

Part of the liquid nitrogen at the top of the high-pressure column ensures its reflux current and the remaining  $\text{N}_2$  liquid together with the nitrogen gas are throttled in a throttling valve to the pressure of the low pressure column and feed in liquid state LPC on the top.

From the HPC base the liquid enriched in  $\text{O}_2$  is throttled and introduced in the middle of the low-pressure column where the distillation process is continued.

Distillation products (separate gases) are discharged from the low-pressure column.

To supplement the cold capacity of the installation a fraction of about 15% of the compressed air is expelled into a holder before being introduced into the low-pressure column.

The simulation of the operation of the cryogenic air separation installation was performed using the ChemSep simulator [106].

#### Air Separation Unit - 2000 t/day Oxygen

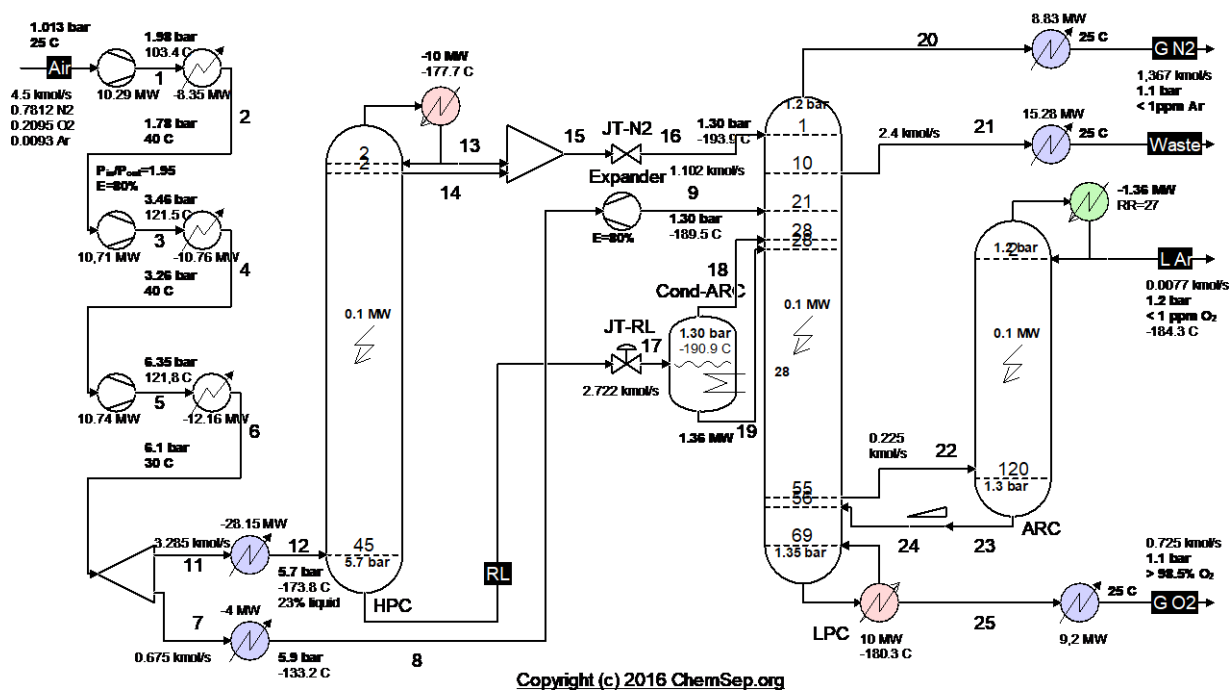


Figure 4.1. Diagram of the cryogenic air separation installation

## 4.2 Exergetic analysis

Looking at the installation as a whole (Fig. 4.1) one can identify the products, the exergetic fuel and the losses of the global system (Fig. 4.2).

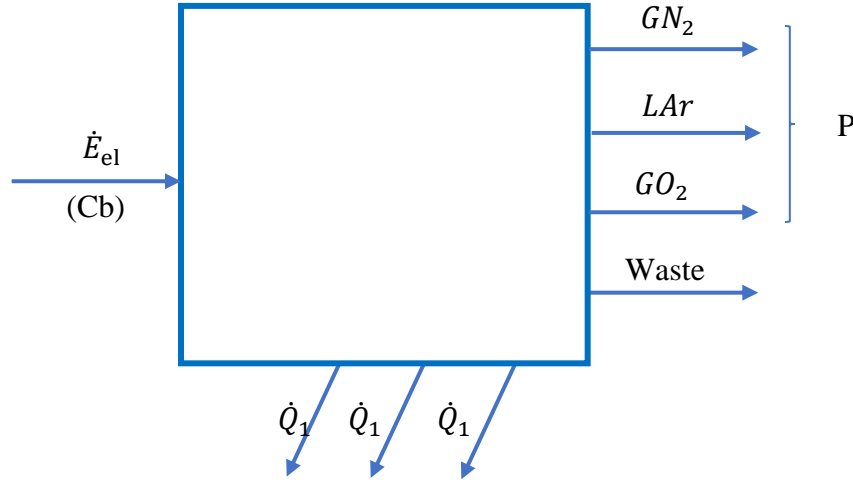


Figure 4. 2. Diagram of interactions with the external environment of the global system of the cryogenic air separation installation

The exergetic performance coefficient of the whole system is :

$$COP_{ex} = \frac{P}{Cb} = \frac{\dot{E}x_{GN_2}^{TOT} + \dot{E}x_{LAr}^{TOT} + \dot{E}x_{GO_2}^{TOT}}{\dot{E}el} \quad (4.1)$$

The terms of the product of the installation are calculated as follows

$$\dot{E}x_{GN_2}^{TOT} = \dot{E}x_{GN_2}^{TM} + \dot{E}x_{GN_2}^{CH} \quad (4.3)$$

$$\dot{E}x_{GN_2}^{TM} = n_{GN_2} \{ \bar{h}_{N_2}(T, p) - \bar{h}_{N_2}(T_0, p_0) - T_0 [ \bar{s}_{N_2}(T, p) - \bar{s}_{N_2}(T_0, p_0) ] \} \quad (4.4)$$

$$\dot{E}x_{GN_2}^{CH} = n_{GN_2} \cdot \bar{R} \cdot T_0 \cdot \ln \frac{r_{N_2}}{r_{N_2}^0} \quad (4.5)$$

The reference state is characterized by  $t_0 = 25^\circ C$ ,  $p_0 = 1,013 \text{ bar}$  and the air composition is  $r_{N_2} = 0,7812$ ;  $r_{O_2} = 0,2095$ ;  $r_{Ar} = 0,0093$ .

Table 4.1. The values for the input compressors power

Compressor	$ \dot{L} $ [kW]
1	10292
2	10712
3	10751
<b>Combustible for the global system Cb</b>	<b>31755</b>

Table 4.2. Values for the exergies of the products

Substance	$\dot{E}_x^{TM}$ [kW]	$\dot{E}_x^{CH}$ [kW]	$\dot{E}_x^{TOT}$ [kW]
$GO_2$	377,4	2752	3129,4
$GN_2$	279	835,8	1114,8
$LAr$	151,5	89,53	241
<b>Product for the global installation P</b>			4485,2

The value of the exergetic coefficient of performance (eq. 4.1) is  $COP_{ex} = 0,14$

To identify the place where losses and destruction take place, the installation is divided into functional areas (Fig. 4.3).

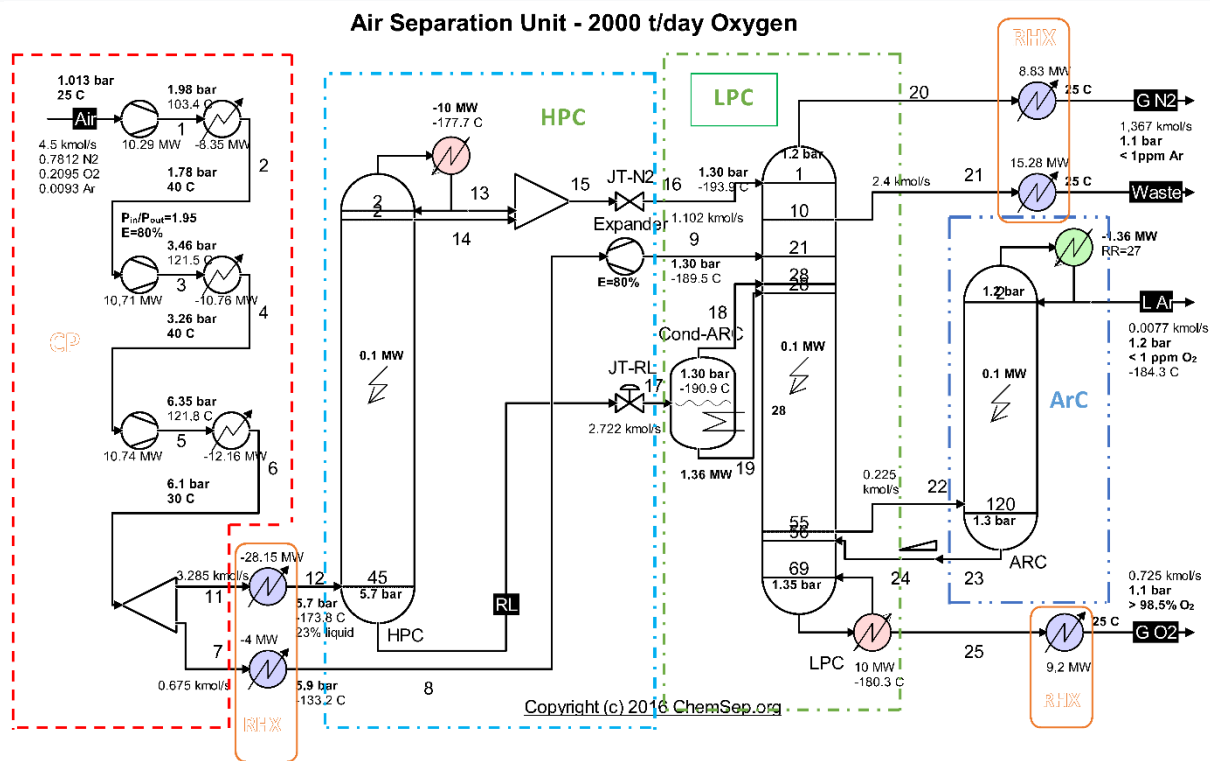


Figure 4.3. Diagram of the cryogenic air separation installation - functional areas

#### 4.3 Compression area

The diagram of the interactions of the compression zone with the outside is presented in figure 4.5.

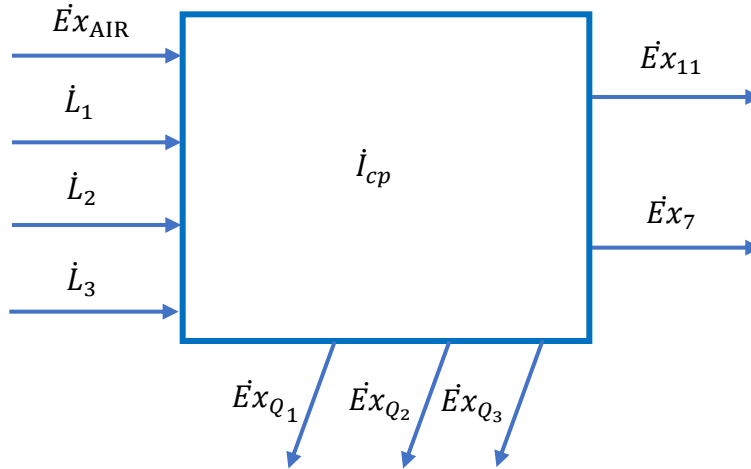


Figure 4.4. Diagram of the interactions of the compression area with the outside

The exergetic balance equation for compression area is:

$$\sum \dot{E}x_i = \sum \dot{E}x_e + i \quad (4.15)$$

In the balance exergetic equation (4.15) both the inlet and outlet exergies are in absolute values.

$$\dot{E}x_{AIR} + |\dot{L}_1| + |\dot{L}_2| + |\dot{L}_3| = \dot{E}x_{11} + \dot{E}x_7 + |\dot{E}x_{Q1}| + |\dot{E}x_{Q2}| + |\dot{E}x_{Q3}| + i \quad (4.16)$$

Equation (4.16) written with an economic tint becomes:

$$Cb_{cp} = P_{cp} + (Pi + I)_{cp} \quad (4.17)$$

Where  $Cb$  is the fuel of the area

$$Cb_{cp} = Cb = |\dot{L}_1| + |\dot{L}_2| + |\dot{L}_3| \quad (4.18)$$

and  $P$  is the product of the area and represents the net increase in its exergy.

$$P_{cp} = \dot{E}x_{11} + \dot{E}x_7 - \dot{E}x_{AIR} \quad (4.19)$$

$$Pi_{cp} = |\dot{E}x_{Q1}| + |\dot{E}x_{Q2}| + |\dot{E}x_{Q3}| \quad (4.20)$$

with the significance of the loss of exergy with the heat evacuated to the outside in the intermediate coolers and the final one of the compression area.

$I$  is the destruction of exergy in the compression process.

Equation (4.17) becomes:

$$|\dot{L}_1| + |\dot{L}_2| + |\dot{L}_3| = (\dot{E}x_{11} + \dot{E}x_7 - \dot{E}x_{AIR}) + |\dot{E}x_{Q1}| + |\dot{E}x_{Q2}| + |\dot{E}x_{Q3}| + i \quad (4.21)$$

For the compression zone the share of exergy losses and destructions in the total fuel consumption of the installation is:

$$Y_{cp} = \frac{(Pi + I)_{cp}}{|\dot{L}_1| + |\dot{L}_2| + |\dot{L}_3|} \quad (4.32)$$

#### 4.4 The high-pressure distillation column (HPC)

The area of the HPC distillation column, separated from the rest of the plant, is shown in Figure 4.3.

The diagram of the interactions of the HPC area with its exterior can be found in figure 4.7

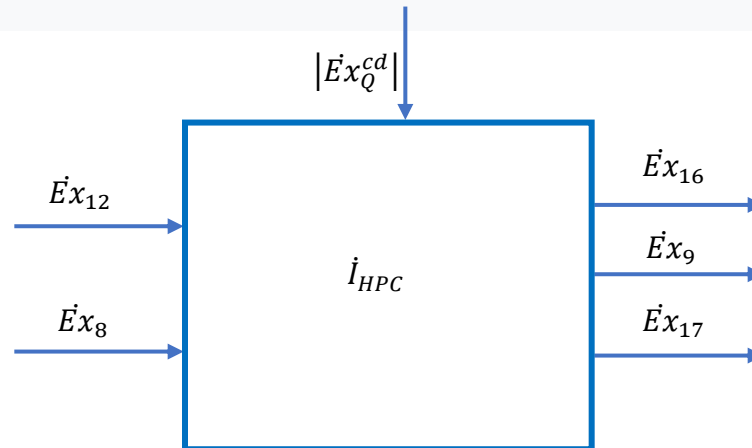


Figure 4.5. Scheme of interactions with the external environment of the area of the high pressure distillation column (HPC)

The effect of heat penetration from the environment is neglected in a first phase and it is considered that the heat exchange with the outside in the HPC is performed only in the condenser. The HPC exergetic balance equation becomes:

$$\dot{E}x_Q^{cd} = \dot{E}x_{16} + \dot{E}x_9 + \dot{E}x_{17} - \dot{E}x_{12} - \dot{E}x_8 + \dot{i} \quad (4.34)$$

To highlight the chemical component of the exergy, the exergy of the substance currents is split into the thermo-mechanical (physical) and the chemical component.

The exergetic balance equation (4.36) becomes:

$$\begin{aligned} |\dot{E}x|_Q^{cd} + \dot{E}x_{12}^{TM} + \dot{E}x_{12}^{CH} + \dot{E}x_8^{TM} + \dot{E}x_8^{CH} = \\ = \dot{E}x_{16}^{TM} + \dot{E}x_{16}^{CH} + \dot{E}x_9^{TM} + \dot{E}x_9^{CH} + \dot{E}x_{17}^{TM} + \dot{E}x_{17}^{CH} + \dot{i} \end{aligned} \quad (4.38)$$

The product is the increase in the chemical exergy on the inlet-outlet path of the distillation column.

$$P_{HPC}^{CH} = \dot{E}x_{16}^{CH} + \dot{E}x_9^{CH} + \dot{E}x_{17}^{CH} - \dot{E}x_{12}^{CH} - \dot{E}x_8^{CH} \quad (4.39)$$

The exergetic coefficient of performance of the HPC becomes:

$$COP_{exCH}^{HPC} = \frac{P_{HPC}^{CH}}{Cb_{HPC}^{CH}} = \frac{\dot{E}x_{16}^{CH} + \dot{E}x_{17}^{CH} - \dot{E}x_{12}^{CH}}{|\dot{E}x|_Q^{cd} + \dot{E}x_{12}^{TM} + \dot{E}x_8^{TM} - \dot{E}x_{16}^{TM} - \dot{E}x_9^{TM} - \dot{E}x_{17}^{TM}} \quad (4.42)$$

Exergy destruction can also be calculated based on the Gouy-Stodola theorem:

$$\dot{I}_{HPC} = T_0 \cdot \dot{S}_{gen}^{HPC} \quad (4.44)$$

Where

$$\begin{aligned} \dot{S}_{gen}^{HPC} &= \sum \dot{S}_e - \sum \dot{S}_i - \frac{\dot{Q}_{cd}}{T_{cd}} = \\ &= \dot{n}_{16} \cdot \bar{s}_{16} + \dot{n}_9 \cdot \bar{s}_9 + \dot{n}_{17} \cdot \bar{s}_{17} - \dot{n}_{12} \cdot \bar{s}_{12} - \dot{n}_8 \cdot \bar{s}_8 + \frac{|\dot{Q}_{cd}|}{T_{cd}} \end{aligned} \quad (4.45)$$

The share of exergy destruction in HPC in the total fuel consumption of the installation is

$$Y_{HPC} = \frac{\dot{I}_{HPC}}{|\dot{L}_1| + |\dot{L}_2| + |\dot{L}_2|} \quad (4.46)$$

#### 4.5 Low pressure distillation column (LPC)

The area of the low pressure distillation column separated from the rest of the installation is presented in figure 4.3.

The diagram of the interactions of the LPC area with its exterior can be found in figure 4.9

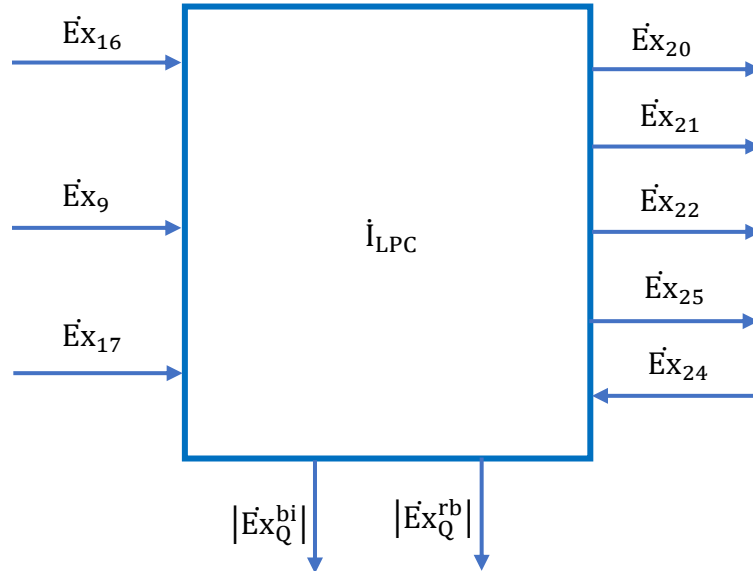


Figure 4.6. Diagram of the interactions of the LPC area with its exterior

The product of the low - pressure column defined as the increase in chemical exergences of the substances passing through the contour of the low- pressure column is:

$$\begin{aligned} P_{LPC}^{CH} &= \\ &= \dot{E}x_{20}^{CH} + \dot{E}x_{21}^{CH} + \dot{E}x_{22}^{CH} + \dot{E}x_{25}^{CH} - \dot{E}x_{16}^{CH} - \dot{E}x_9^{CH} - \dot{E}x_{17}^{CH} - \dot{E}x_{24}^{CH} + |\dot{E}x|_Q^{bi} + |\dot{E}x|_Q^{rb} \end{aligned} \quad (4.54)$$

Low pressure column fuel when the product is characterized only by upgrading of chemical exergies is defined by decreasing the thermo-mechanical exergies of the processed currents:

$$Cb_{LPC}^{CH} = \dot{E}x_{16}^{TM} + \dot{E}x_9^{TM} + \dot{E}x_{17}^{TM} + \dot{E}x_{24}^{TM} - \dot{E}x_{20}^{TM} - \dot{E}x_{21}^{TM} - \dot{E}x_{22}^{TM} - \dot{E}x_{25}^{TM} \quad (4.55)$$

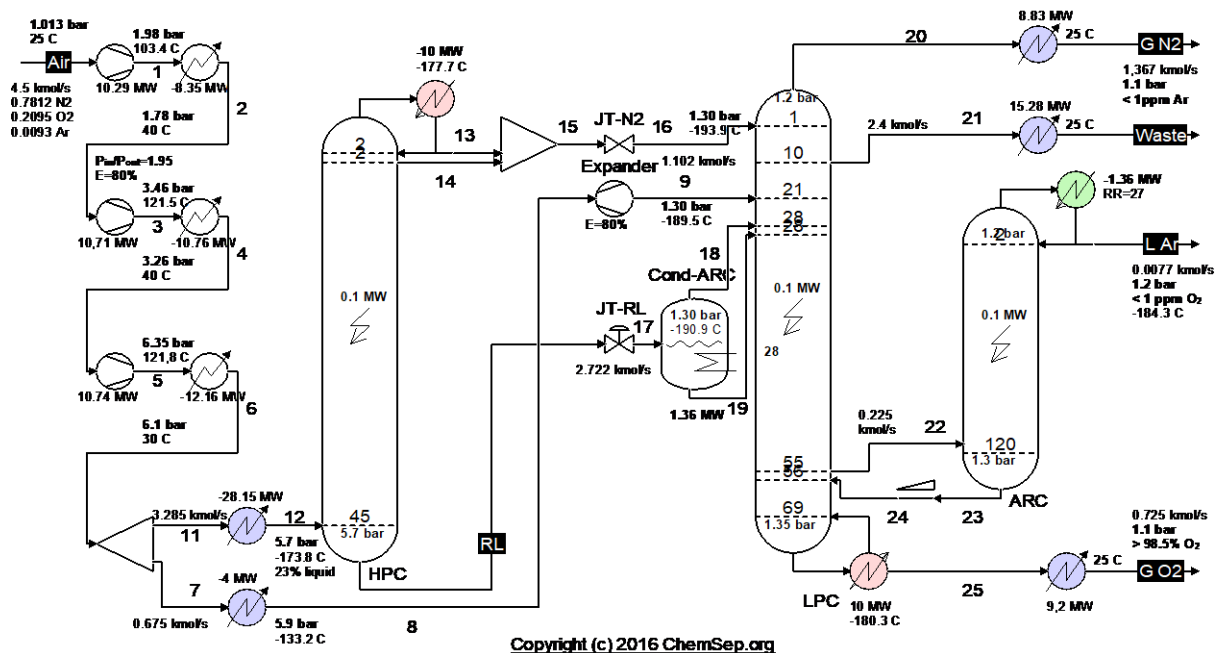
The exergy destruction in the LPC is:

$$\dot{i}_{LPC} = Cb_{LPC}^{CH} - P_{LPC}^{CH} \quad (4.56)$$

#### 4.6 Results and discussion:

The modeling of the operation of the air separation system called for the calculation of the separation columns at the ChemSep simulator.

#### Air Separation Unit - 2000 t/day Oxygen



Stream	G N2	Waste	L Ar	25	G O2	Unit
Pressure	1.1	1.11956521739	1.2	1.35	1.25	bar
Temperature	25	25	-184.33195653	-180.321687086	25	°C
Flow rate	1.36717025164	2.4	0.00772506877116	0.725104679833	0.725104679833	kmol / s
Mole frac. Nitrogen	0.999981812771	0.895106083321	5.15432166759e-09	2.65309385707e-17	2.65309385707e-17	
Mole frac. Oxygen	4.77434787231e-06	0.095214732964	7e-07	0.985	0.985	
Mole frac. Argon	1.34128809187e-05	0.0096791837146	0.999999294846	0.015	0.015	
Flow Nitrogen	1.3671453866	2.14825459997	3.98174893508e-11	1.9237707718e-17	1.9237707718e-17	kmol / s
Flow Oxygen	6.527346382e-06	0.228515359114	5.40754813981e-09	0.714228109635	0.714228109635	kmol / s
Flow Argon	1.83376917809e-05	0.023230040915	0.00772506332379	0.0108765701975	0.0108765701975	kmol / s
Enthalpy	-8.45380637756	-8.83755993361	-10771.5285056	-12706.3042166	-11.7951039983	kJ / kmol
Entropy	-0.705339485856	2.20508647215	-98.5705176391	-107.998082668	-1.12829829892	kJ / kmol K
Volume	0.0225248346209	0.0221297066151	2.52154589397e-05	2.51887491908e-05	0.0198088484998	m <sup>3</sup> / mol
Vapor phase						
Mole phase fraction	1	1	0	0	1	
Liquid phase						
Mole phase fraction			1	1		

Stream	Feed1	V.Feed1	L.Feed1	Top	Bottom	Sidestream
Stage	45	45	45	1	45	2
Pressure (bar)	5.70100	5.70000	5.70000	5.60000	5.70000	5.60000
Vapour Fraction (-)	0.770598	1.00000	0.000000	0.000000	0.000000	1.00000
Temperature (K)	99.4000	99.3977	99.3977	95.4226	98.5931	95.4226
Enthalpy (J/kmol)	-7.261E+06			-1.097E+07	-1.124E+07	-6.202E+06
Entropy (J/kmol/K)	-55448.4			-99433.7	-94491.6	-49386.7
Total molar flow (kmol/s)	3.82500	2.94758	0.877423	1.07098	2.72283	0.0311901
Total mass flow (kg/s)	110.768	84.8636	25.9048	30.0014	79.8933	0.873728
Vapour std.vol.flow (m3/s)	70.2343	69.8275				0.738882
Liquid std.vol.flow (m3/s)	0.0279116		0.0284545	0.0372250	0.0891392	
Mole flows (kmol/s)						
Nitrogen	2.98809	2.42115	0.566936	1.07098	1.88592	0.0311901
Oxygen	0.801337	0.501918	0.299420	1.2613E-10	0.801337	3.6733E-12
Argon	0.0355725	0.0245050	0.0110675	7.4968E-07	0.0355717	2.1833E-08
Mole fractions (-)						
Nitrogen	0.781200	0.821405	0.646137	0.999999	0.692632	0.999999
Oxygen	0.209500	0.170281	0.341249	1.1777E-10	0.294303	1.1777E-10
Argon	0.00930000	0.00831362	0.0126136	7.0000E-07	0.0130643	7.0000E-07
Mass flows (kg/s)						
Nitrogen	83.7054	67.8238	15.8816	30.0014	52.8303	0.873727
Oxygen	25.6420	16.0609	9.58114	4.0360E-09	25.6420	1.1754E-10
Argon	1.42105	0.978928	0.442123	2.9948E-05	1.42102	8.7218E-07
Mass fractions (-)						
Nitrogen	0.755679	0.799210	0.613074	0.999999	0.661260	0.999999
Oxygen	0.231492	0.189255	0.369859	1.3452E-10	0.320953	1.3452E-10
Argon	0.0128290	0.0115353	0.0170672	9.9823E-07	0.0177865	9.9823E-07
Combined Feed fractions (-)						
Nitrogen	1.00000	0.810268	0.189732	0.358416	0.631146	0.0104381
Oxygen	1.00000	0.626350	0.373650	1.5740E-10	1.00000	4.5839E-12

#### 4.6.1 Compression area

The increase in air pressure is achieved in a step-by-step compression system with intermediate cooling between steps and final cooling.

To evaluate the performance of the area, attention was focused on exergy losses with heat discharged to the outside in the coolers of the compression system and on the destruction of exergy due to the irreversibility of compression processes.

The product of the area is the net increase in the total exergy of the air between inlet and outlet and the fuel (resource used) is represented by electricity to drive the compressors.

Table 4.3. The values of the total exergences of the air currents, of the driving power of the compressors and of the exergies of the heat evacuated by the cooling system

Curent of exergy	Exergy[MW]
AIR	0
$ \dot{L}_1 $	10,29
$ \dot{L}_2 $	10,71
$ \dot{L}_3 $	10,75
$ \dot{E}x_{Q_1}  + \dot{I}_{\Delta p_1}$	-2,3
$ \dot{E}x_{Q_2}  + \dot{I}_{\Delta p_2}$	-2,32
$ \dot{E}x_{Q_3}  + \dot{I}_{\Delta p_3}$	-2,161
$\dot{E}x_6^{TOT}$	-20,015
$\dot{I}_{cp} = \sum \dot{E}x_i - \sum \dot{E}x_e$	<b>4,954</b>

**Table 4.4.** Losses with heat exergies discharged into the coolers of the compression stages

Cooler	Loos with the discharged heat $ \dot{E}_{xQ}  + \dot{I}_{\Delta p}$ [MW]
1	2,3
2	2,32
3	2,161
<b>Total <math>P_{iQ}</math></b>	<b>6,781</b>

Exergy losses and destructions in the compression area include:

$$\dot{I}_{Z,cp} = \dot{I}_{cp} + P_{iQ} = 4,958 + 6,781 = 11,739 \text{ MW}$$

The share of energy losses and destruction in the compression zone in the fuel consumption of the global installation is:

$$Y_{cp} = \frac{\dot{I}_{Z,cp}}{|\dot{L}_1| + |\dot{L}_2| + |\dot{L}_3|} = \frac{11,739}{31,75} = 0,37$$

It follows that 37% of the electricity consumption of the cryogenic air separation plant is lost or destroyed in the compression zone.

#### 4.6.2 High pressure distillation column

If the product and fuel are defined considering the total exergies which, in addition to the chemical part, also consider the pressure and temperature of each substance stream, elements which count in  $P_{HPC}$  becomes fuel the results recorded in Table 4.9 are obtained.

Table 4.5. Values for product, fuel, and coefficient of performance when considering that the purpose of HPC is to increase total exergy by separating streams of substance

$P_{HPC}^{TOT}$ [MW]	$Cb_{HPC}^{TOT}$ [MW]	$COP_{ex,HPC}^{TOT}$ %
42,86	68,397	62,66

To calculate the exergy destruction in the high-pressure column HPC, the Gouy-Stodola theorem was used in which the entropy values calculated with ChemSep were used. (eq. 4.45). That leads to a share of exergy destruction in the overall consumption of the installation (eq. 4.46) of  $Y_{HPC} = 8.3\%$

## CHAPTER 5. EXERETIC ANALYSIS OF THE COMPRESSION ZONE

The compression zone of the cryogenic air separation system consists of three compression stages and three heat exchangers, of which two intermediate and one final cooler.

### 5.1 Compression stage

Figure 5.1 shows in the diagram T-s the compression process in the first stage of the compressor.

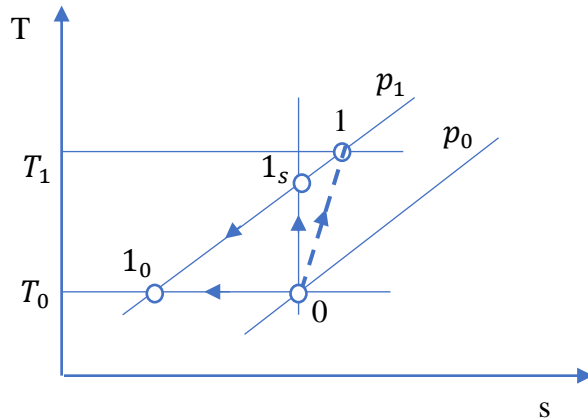


Figure 5.1. Representation in the T-s diagram of the first stage compression process

The exergetic balance equation of the compression stage, written for 1 kmol of air becomes:

$$\sum \bar{e}x_q = \Delta \bar{e}x + \bar{l}_{cp} + \sum \bar{i} \quad (5.1)$$

$$|\bar{l}_{cp}| = \bar{l}_{cpT_0} + \bar{i}_{\Delta T} + \bar{l}_{cp} \quad (5.11)$$

$$COP_{ex}^{cp} = \frac{|\bar{l}_{cpT_0}|}{|\bar{l}_{cp}|} = 1 - \frac{\bar{i}_{\Delta T} + \bar{l}_{cp}}{|\bar{l}_{cp}|} \quad (5.12)$$

$$COP_{ex}^{cp} = \frac{T_0 \cdot \bar{R} \cdot \ln \pi}{\bar{h}_1(T_1) - \bar{h}_0(T_0)} = \frac{T_0 \cdot \bar{R} \cdot \ln \pi}{\bar{h}_1(T_0, \pi, \eta_{s,cp}) - \bar{h}_0(T_0)} \quad (5.17)$$

It is interesting to follow the variation of the coefficient of exergetic performance of the compressor and the weights of the exergy losses to the variation of the compression ratio and the isentropic compression efficiency.

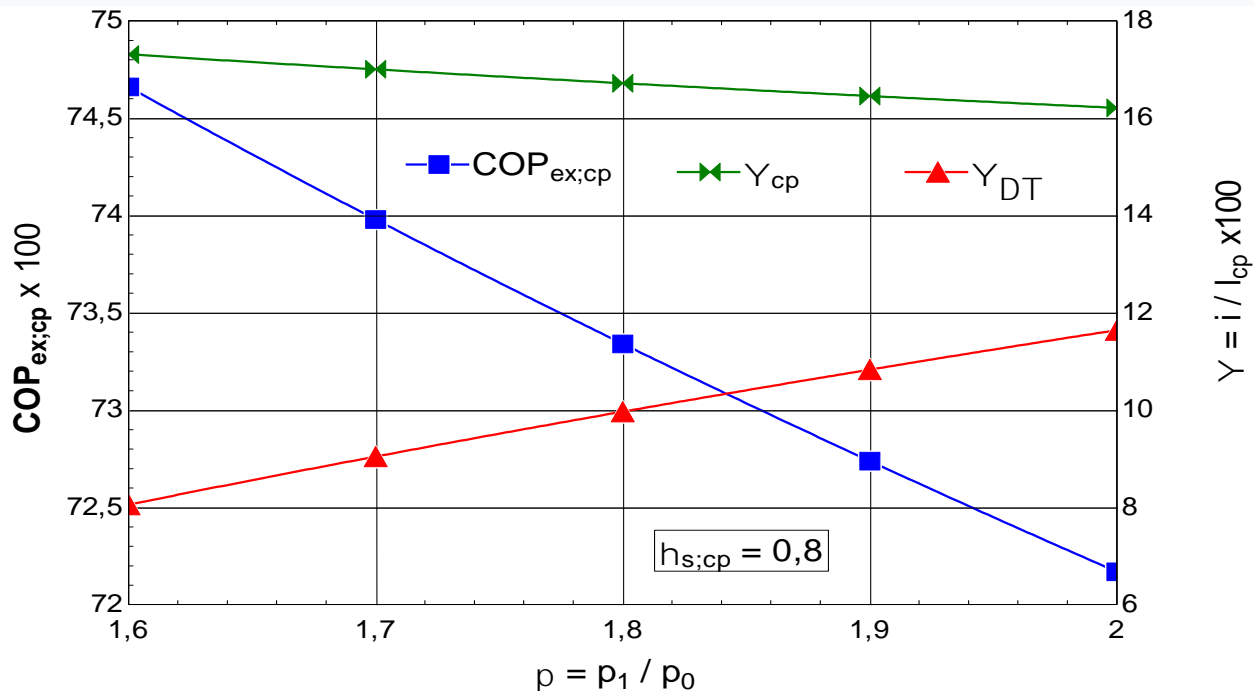


Figure 5.2. Exergetic coefficient of performance of the compression stage and share of exergy destructions in the mechanical drive power as a function of the compression ratio

În cazul creșterii raportului de comprimare pe treaptă, coeficientul de performanță exergetică scade datorită creșterii nedorite a temperaturii aerului refulat ( $\psi_{\Delta T}$ ) care este mai pronunțată decât scăderea ponderii distrugerii de exergie cauzată de frecările interne ( $\psi_{cp}$ ) (Fig. 5.2)

## 5.2 Choice of intermediate chillers and final cooler on the basis of optimum entropy generation (optimum exergy destruction)

The destroyed exergy in a heat exchanger can be calculated based on the Gouy-Stodola theorem:

$$\dot{i} = T_0 \cdot \dot{S}_{gen} \quad (5.19)$$

### Exergy destruction in the cooler

If we consider only the destruction of exergy caused by the transfer of heat to the cooling medium (water and finally the cooling tower) considered to be a good approximation of the environment, its expression is:

$$\dot{i}_{\Delta T} = \dot{Q} \cdot T_0 \frac{T_c - T_r}{T_c \cdot T_r} = \dot{Q} \left( 1 - \frac{T_r}{T_c} \right) \quad (5.40)$$

Reporting the relation (5.40) to  $Q$  we obtain a dimensionless number that we will call NEU - the number of destroyed exergy units.

$$NEU = \frac{\dot{i}_{\Delta T}}{\dot{Q}} = \left( 1 - \frac{T_r}{T_c} \right) \quad (5.41)$$

The first intermediate cooler of the compression zone is characterized by a ratio of the calorific capacities of the two currents

$$C = \frac{C_{min}}{C_{max}} = \frac{C_c}{C_r} = 0,14$$

The NEU -  $\varepsilon$  diagram constructed based on the relations (5.41; 5.44-46) is presented in figure 5.6.

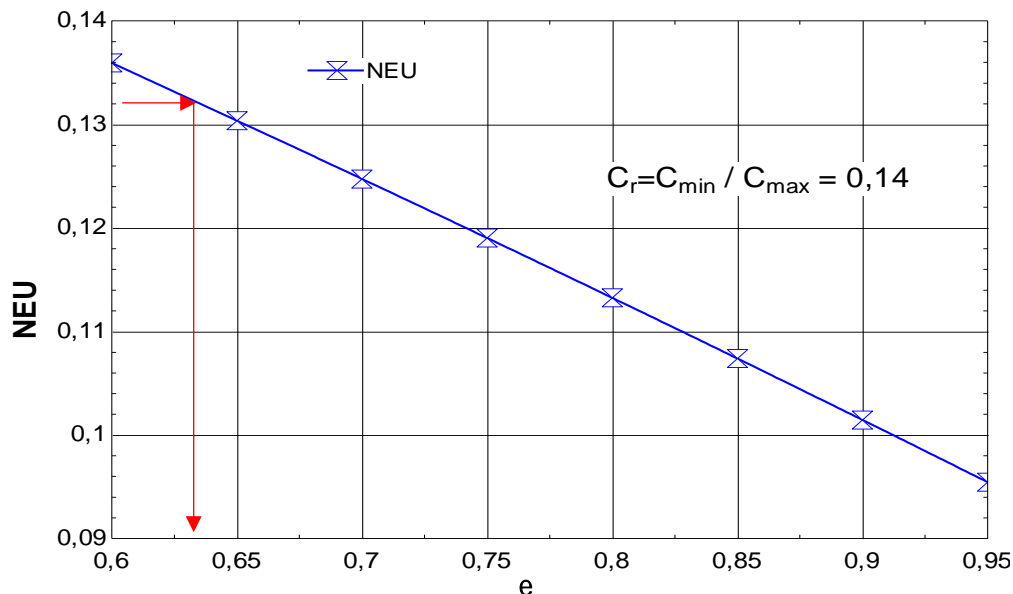


Figure 5.3. Number of NEU destroyed exergy units depending on the efficiency of the first intermediate chiller

The average thermodynamic temperatures of the air (hot stream) in the first cooler and of the cooling water are:

$$T_{c_1} = 343,7 \text{ K} \quad \text{și} \quad T_{r_1} = 298,33 \text{ K} \quad , \text{ to which they correspond (eq. 5.41) } NEU_1 = 0.132$$

From figure 5.6 the value  $NEU_1 = 0.132$  corresponds to a thermal efficiency  $\varepsilon_1 = 0,63$

Knowing the thermal efficiency of the heat exchanger for a specified number of destroyed exergy units can determine the number of NTU heat transfer units and finally the conductance (kA) of the heat exchanger based on the relation:

$$NTU = \frac{k \cdot A}{C_c} \quad (5.33)$$

## CHAPTER 6. ATTEMPTS FOR INCREASING THE PERFORMANCE OF CRYOGENIC AIR SEPARATION INSTALLATIONS

### 6.1 The heat recovery potential evacuated by the cryogenic air separation installation from the Galati Steel Plant

The exergetic analysis of the installation highlights the fact that the compression stage represents an area with a major destruction of exergy (electricity); 37% of the electricity consumption of the global installation is dissipated in the irreversible processes of the compression zone.

From this exergy consumption more than half (21% of the global consumption) represents the loss with the exergy of the heat evacuated to the external environment.

Due to the relatively low average temperature level (70-80oC) of the heat discharged by the compressor cooling system, a viable solution is to transform this heat into mechanical work (electricity) using a Rankine cycle running on organic fluids.

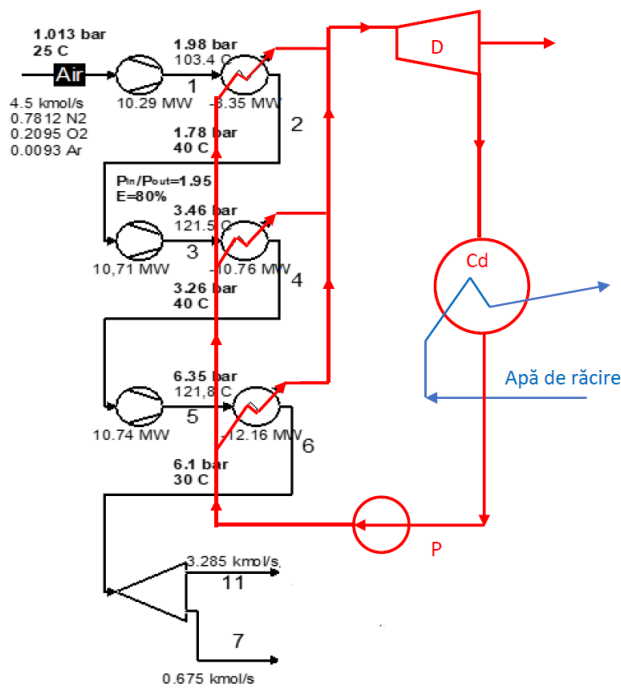


Figure 6.1 . Scheme of use of ORC for intermediate and final cooling of compressors

6.3.1 ORC cycle with non-negative vapor saturation curve slope without vapor overheating at the inlet to the holder and without internal recuperator heat exchanger

The diagram of the ORC system is presented in figure (6.13 a) and the representation of the cycle in the diagram T-s, in figure (e 13.b).

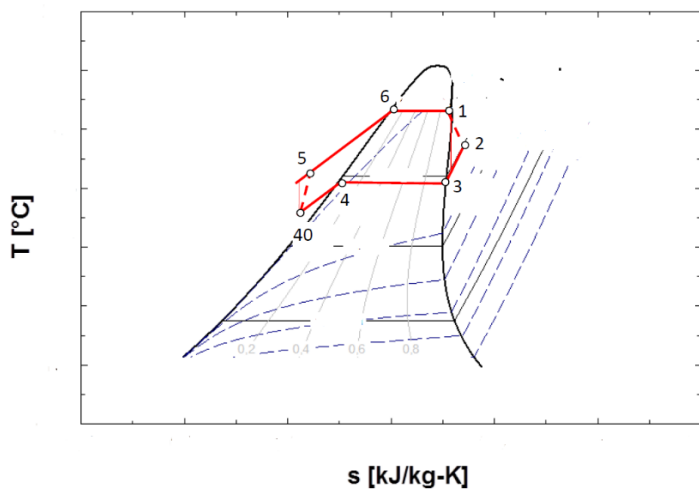
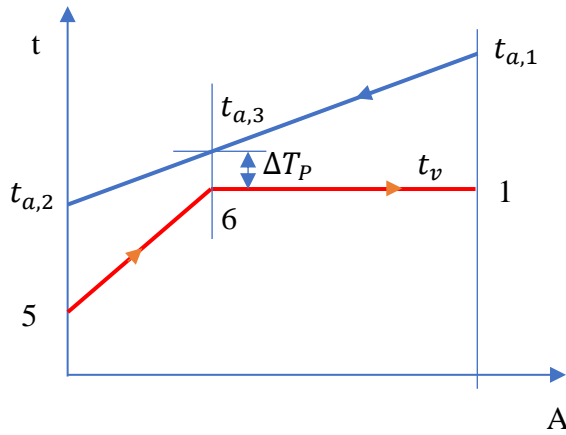


Figure 6.2. Representation in the T-s diagram of the ORC cycle without overheating of the vapors at the inlet of the holder and without internal recuperative heat exchanger

6.3.4 Mathematical modeling of the ORC cycle

In designing the mathematical model, the main elements are the choice of vaporization and condensation temperatures

- The vaporization temperature is imposed by the minimum temperature difference in the vaporizer (Pinch temperature difference) that occurs at the end of heating the liquid in the vaporizer and the beginning of vaporization.



**Figure 6.3.** Temperature - Area (T-A) diagram of the ORC cycle evaporator without overheating and without internal recovery exchanger

- Condensation temperature is determined by the temperature of the cooling water and the minimum temperature difference in the condenser (temperature difference at Pinch  $\Delta T_P$ )

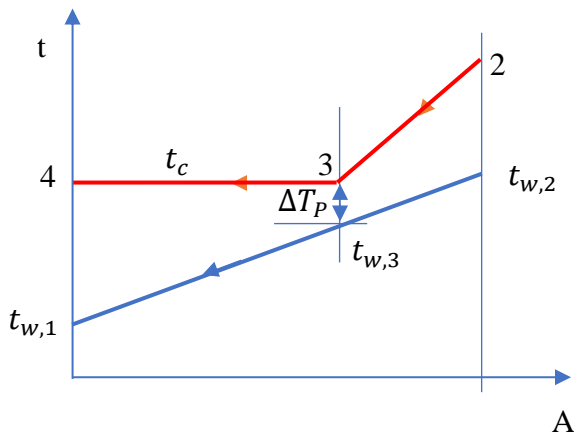


**Figure 6.4.** Temperature - Area (T-A) diagram of the ORC cycle condenser without overheating and without internal recovery

## 6.4 Exergetic analysis

The exergetic balance equation for the cycle without overheating and without internal recuperative heat exchanger (fig. 6.13) is:

$$\dot{Ex}_Q^{T_{a,1-2}} = \dot{W} + |\dot{Ex}|_Q^{T_2-4} + \dot{I}_{\Delta T,v} + \dot{I}_D + \dot{I}_P \quad (6.47)$$

Exergetic efficiency

$$\eta_{ex} = \frac{\dot{W}}{\dot{Ex}_Q^{T_{a,1-2}}} \quad (6.52)$$

The share of an exergy destruction in the exergy of the heat available for recovery

$$\psi = \frac{\dot{I}}{\dot{Ex}_Q^{T_{a,1-2}}} \quad (6.53)$$

### 6.5.1 Study of the performance of the ORC cycle operating with R-245fa

*ORC system with R-245fa without overheating and without internal recovery exchanger (fig.6.13).*

The results of the mathematical modeling based on the exergetic analysis of the ORC cycle operation with R-245fa, without overheating and without internal heat exchanger, are presented in table 6.4.

Table 6.1. Energy and exergetic quantities for the ORC cycle with R-245fa, without overheating and without internal heat exchanger (IHx)

$t_v$	$\eta_{ex}$	$W$	$W_D$	$W_P$	$m_{orc}$	$t_v$	$\Psi_v$	$\Psi_{cd}$	$\Psi_D$	$t_2$	$t_5$
[°C]	[%]	[kW]	[kW]	[kW]	[kg/s]	[°C]	[%]	[%]	[%]	[°C]	[°C]
35	21,44	1172	1187,82	15,82	146,9	35	56,4	18,36	3,675	23,09	15,06
38	25,25	1380	1400	20	145,4	38	52,02	18,26	4,324	23,78	15,08
41	28,92	1580	1604	24	143,9	41	47,81	18,16	4,946	24,49	15,09
44	32,45	1773	1801,56	28,56	142,5	44	43,74	18,07	5,543	25,21	15,11

The exergy destructions with the highest weights have the processes from vaporizer ( $\Psi_v$ ) and condenser-subcooler ( $\Psi_{cd}$ ). Increasing the temperature of the agent ( $T_v$ ) that takes over the recovered heat, reduces the energy of this transfer process.

The increase of the temperature of the ORC agent when taking over the heat recovered from the cooling system of the ASU compression stage can be done by recovering in an internal exchanger the heat of the vapors from the exit of the holder under the conditions where the temperature difference  $t_2-t_5$  allows this ( Fig.6.14).

Table 6. 2. Energy and exergetic quantities for the ORC cycle with R-245fa, without overheating but with internal heat exchanger (IHx)

$t_v$	$\eta_{ex}$	$W$	$m_{orc}$	$\Psi_v$	$\Psi_{cd}$	$\Psi_D$	$t_2$	$t_5$	$t_7$	$t_8$
[°C]	[%]	[kW]	[kg/s]	[%]	[%]	[%]				
35	21,7	1186	148,6	56,03	18,31	3,719	23,09	15,06	20,46	16,95
38	25,62	1400	147,5	51,51	18,18	4,386	23,78	15,08	20,57	17,38
41	29,41	1607	146,4	47,14	18,06	5,029	24,49	15,09	20,67	17,83
44	33,08	1808	145,3	42,9	17,93	5,651	25,21	15,11	20,78	18,29
47	36,64	2002	144,3	38,79	17,81	6,251	25,95	15,13	20,89	18,75

The increase of the mechanical power offered by the ORC cycle at the decrease the exergy destruction in the evaporator, by internal recovery with consequence of increasing the temperature of the ORC agent at the entrance to the vaporizer in the heating zone, urges us to try to further reduce this destruction by overheating.

The results of the comparative analysis for the three schemes - without overheating and without internal recovery exchanger, without overheating and with internal recovery exchanger and finally the scheme with overheating and internal recovery exchanger are presented in table 6.7.

Tabel 6.3. Comparative analysis - Energy and exergetic quantities for different types of ORC cycles with R-245fa, ( $t_v = 45^\circ\text{C}$ )

Cycle type	$\eta_{\text{ex}}$	$\dot{W}$	$\dot{m}_{\text{orc}}$	$\Psi_v$	$\Psi_{\text{inc}}$	$\Psi_{\text{zvap}}$	$\Psi_{\text{si}}$	$\Psi_{\text{cd}}$	$\Psi_{\text{D}}$
	[%]	[kW]	[kg/s]	[%]	[%]	[%]	[%]	[%]	[%]
Without IHX without overheating	33,6	1836	142	42,42	4,803	37,61	-	18,04	5,737
With IHX without overheating	34,28	1873	144,96	41,52	3,743	37,77	-	17,89	5,853
With IHX and overheating $\Delta T_{\text{sh}}=10\text{K}$	35,51	1940	143,6	39,59	1,916	34,4	3,265	17,87	5,856

The comparative analysis presented in Table 6.7 shows the decreasing trend of exergy destruction in the vaporizer as the temperature of the ORC fluid increases and the temperature difference between the air to be cooled and the ORC fluid that takes over the heat decreases. This fact is also confirmed by studies [119], [120].

In the conditions imposed by the recovery of the heat evacuated from the compression stage of the cryogenic air separation installation from the Galati Iron and Steel Works and following the comparative study using different organic fluids, the following resulted (Table 6.11)

Table 6.4. Performance parameters of ORC cycles with working with different working agents

Fluid ORC	$\dot{W}$ [kW]	$\dot{m}$ [kg/s]	$\eta_{\text{ex}}$ [%]	Operating conditions
<b>R-245fa</b>	1940	143,6	35,51	Cycle with overheating $\Delta T_{\text{si}}=10\text{K}$ and internal heat exchanger (IHX) $t_v=45^\circ\text{C}$ ;
<b>n-pentan</b>	1956	75,06	35,8	Cycle with overheating $\Delta T_{\text{si}}=10\text{K}$ and internal heat exchanger (IHX) $t_v=45^\circ\text{C}$ ;
<b>R-123</b>	1963	160,5	35,92	Cycle with overheating $\Delta T_{\text{si}}=10\text{K}$ 10K and internal heat exchanger (IHX) $t_v=45^\circ\text{C}$ ;
<b>R717</b>	1991	23,53	36,43	Cycle with overheating $\Delta T_{\text{si}}=30\text{K}$ and without internal heat exchanger $t_v=45^\circ\text{C}$

## Final conclusions

The study of optimization of gas separation processes and of the cryogenic gas separation installation, as a whole, based on the principles of exergetic analysis, represents an original contribution of the doctoral thesis.

The knowledge of the values of exergy of energy-carrying currents from a mechanical, thermal and chemical point of view allowed to identify dissipative areas with high usable energy consumption (exergy) identifying original possibilities to reduce distractions or recover usable energy losses transferred to the environment.

The solution and study of heat recovery from the compression stage using ORC cycles is an original contribution.

The recovery of the heat evacuated when cooling the air in the compression stage of the cryogenic air separation installation on the platform of the Galati Steel Plant with the help of an ORC cycle and its transformation into electricity is a viable solution. This can reduce the total electricity consumption for driving the compressors by 6%.

### Published articles

**S. Bucsa**, D. Dima, A. Serban, M. F. Stefanescu, V. Popa, and A. Dobrovicescu, “Heat exchanger design based on minimum entropy generation,” *IOP Conf. Ser. Mater. Sci. Eng.*, vol. 595, no. 1, 2019, doi: 10.1088/1757-899X/595/1/012020.

D. Dima, **S. Bucsa**, C. Ionita, E. E. Vasilescu, A. Dobrovicescu, and E. Niculae, “Heat transfer characteristics of a gas cooler,” *IOP Conf. Ser. Mater. Sci. Eng.*, vol. 595, no. 1, 2019, doi: 10.1088/1757-899X/595/1/012028.

**Bucșă S.**, Năstase G., Șerban A., Ciocan M., Drughean L., “Cooling and dehumidification systems used in air separation”, 19 th *International Multidisciplinary Scientific GeoConference Surveying Geology and Mining Ecology Management, SGEM 2019*, Volume 19, Issue 6.1, Pages 139 – 144, ISSN 13142704, ISBN 978-619740876-8, DOI 10.5593/sgem2019/6.1/S24.018

Serban, [A.](#), Stefanescu, [M-F](#), Nastase, [G.](#), Ciocan, [M.](#), **Bucsa, S.**, Dobrovicescu, A., [Exergetic „Analysis of a Cogeneration System for Cooling and Heating”, 2018 UBT INTERNATIONAL CONFERENCE](#), PP 26-31 . DOI 10.33107/ubt-ic.2018.150, <https://knowledgecenter.ubt-uni.net/cgi/viewcontent.cgi?article=1772&context=conference>

**Key words** : cryogenic separation of air, exergetic analysis, heat recovery, organic Rankine cycle (ORC)

### Bibliografie

- [7] Y. E. Yuksel, M. Ozturk, and I. Dincer, “Analysis and assessment of a novel hydrogen liquefaction process,” *International Journal of Hydrogen Energy*, vol. 42, no. 16. pp. 11429–11438, 2017, doi: 10.1016/j.ijhydene.2017.03.064.
- [8] M. Asadnia and M. Mehrpooya, “A novel hydrogen liquefaction process configuration with combined mixed refrigerant systems,” *International Journal of Hydrogen Energy*, vol. 42, no. 23. pp. 15564–15585, 2017, doi: 10.1016/j.ijhydene.2017.04.260.

- [26] G. Chen, "Configuration of air separation unit for steelworks," *Gas.Sep.*, vol. 1, p. 4, 2005.
- [27] L. Tong *et al.*, "Exergy and energy analysis of a load regulation method of CVO of air separation unit," *Appl. Therm. Eng.*, vol. 80, pp. 413–423, 2015, doi: 10.1016/j.applthermaleng.2015.01.074.
- [51] M. Mansoury, S. Jafarmadar, and S. Khalilarya, "Energetic and exergetic assessment of a two-stage Organic Rankine Cycle with reactivity controlled compression ignition engine as a low temperature heat source," *Energy Convers. Manag.*, vol. 166, no. November 2017, pp. 215–232, 2018, doi: 10.1016/j.enconman.2018.04.019.
- [52] V. Badescu, M. H. K. Aboaltaboq, H. Pop, V. Apostol, M. Prisecaru, and T. Prisecaru, "Design and operational procedures for ORC-based systems coupled with internal combustion engines driving electrical generators at full and partial load," *Energy Convers. Manag.*, vol. 139, pp. 206–221, 2017, doi: 10.1016/j.enconman.2017.02.046.
- [119] Y. Dai, J. Wang, and L. Gao, "Parametric optimization and comparative study of organic Rankine cycle (ORC) for low grade waste heat recovery," *Energy Convers. Manag.*, vol. 50, no. 3, pp. 576–582, 2009, doi: 10.1016/j.enconman.2008.10.018.
- [120] A. Landelle, N. Tauveron, P. Haberschill, R. Revellin, and S. Colasson, "Organic Rankine cycle design and performance comparison based on experimental database," *Appl. Energy*, vol. 204, pp. 1172–1187, 2017, doi: 10.1016/j.apenergy.2017.04.012.